PHYSICAL REVIEW A VOLUME 32, NUMBER 3 SEPTEMBER 1985

# Generation and detection of squeezed states of light by nondegenerate four-wave mixing in an optical fiber

M. D. Levenson, R. M. Shelby, and A. Aspect
*IBM Research Laboratory, San Jose, California 95193*

M. Reid and D. F. Walls
*University of Waikato, Hamilton, New Zealand*

(Received 22 April 1985)

Nondegenerate four-wave mixing in a single-mode optical fiber is proposed as a method of squeezed state generation. An analysis of the near-degenerate mixing process for forward propagation in realistic fibers is presented along with the theory of an experimentally feasible detection strategy. The effects of the quantum nature of the optical nonlinearity and absorption are modeled by treating the fiber medium as a collection of anharmonic oscillators. Methods of suppressing undesired effects such as stimulated Brillouin scattering are presented as is a technique for providing the phase-shifted local oscillator wave necessary for the detection of squeezing. Preliminary experiments on fiber characterization and the detection of four-wave parametric fluorescence are described.

## I. INTRODUCTION

Quantum noise theory predicts states of optical radiation in which the fluctuations are not distributed uniformly in phase, as in a coherent state, but rather show less fluctuations in one phase quadrature and more in the orthogonal quadrature.[1–3] Such "squeezed states" of light are predicted to yield quantum-limited detection sensitivity well above the standard quantum limit in a variety of homodyne and heterodyne experiments. While various proposals have been made for methods of generating such states, so far squeezed states have eluded experimental realization. (For preliminary reports on current experiments, see Refs. 4–6.) This paper proposes a new class of squeezed-state generation devices based upon the third-order nonlinearity of single-mode optical fibers. The difficulties inherent in such generation schemes are different from and perhaps more tolerable than those involving the nonlinearities of isolated atoms and nonlinear crystals.

The history of the squeezed-states field is one in which practical and fundamental difficulties overlooked in initial proposals later proved intractable enough to prevent experimental progress. Originally, squeezed states were called "two-photon coherent states" because of the expectation that a two-photon laser operating well above threshold would produce such radiation.[2] It was later realized that spontaneous emission would mask any squeezing produced by such a laser even if a near-degenerate two-photon laser could be operated.[7,8] Later proposals involved parametric amplification[9,10] (or second-harmonic generation[11,12]) in crystals showing a second-order optical nonlinearity.[13] Photorefractive-index damage and low-frequency light scattering in crystals needed in such experiments and the incompatability of available laser and detector technologies seem to make such methods prohibitively difficult at present.

Recent research has focused on degenerate four-wave mixing as a method of demonstrating squeezed states.[14–21] The main conceptual difficulty has been to create a squeezing effect large enough to detect using a process that is intrinsically very weak in all transparent media. Atomic systems—where near-resonant transitions enhance the optical nonlinearity—have attracted particular attention, as has the possibility of enclosing the medium in a single-port cavity.[21–23] Detailed calculations and initial experiments for the near-resonant case have demonstrated the importance of noise arising from the inadvertent creation of an excited-state population.[18,21] While squeezed states may yet be demonstrated using an atomic medium, the medium and laser parameters necessary to produce a detectable reduction in quantum noise in the presence of nonideal noise from the interaction itself are rather beyond current technology. We were therefore led to consider extreme off-resonant interactions and to recover a detectable squeezing effect by tight focusing, high density, and long interaction lengths. Such requirements led naturally to the proposal to use an optical fiber. Preliminary experiments, however, revealed difficulties unique to the fiber geometry.

Section II of this paper outlines the theory of four-wave mixing (4WM) in an optical fiber in sufficient detail to calculate the parameters needed for squeezing. Those parameters are shown to correspond to the "ideal-noise" case of an ensemble of anharmonic oscillators driven far off-resonance. The heterodyne-homodyne detection of squeezed states produced by nondegenerate four-wave mixing is then described. Deleterious effects due to acoustic interactions in the fiber—principally the stimu-

 ©1985 The American Physical Society

lated Brillouin effect—are described and methods proposed for suppressing them.

Section IV describes a proposed experiment for generating squeezed states in an optical fiber employing a traveling-wave geometry. A second experiment using a ring resonator will be the subject of a later paper. Tests of experimental feasibility will be described and discussed.

## II. SQUEEZED-STATE GENERATION AND DETECTION WITH A SINGLE-MODE OPTICAL FIBER

The optical fibers which are used in our experiments consist of $\sim$90-$\mu$m-diam cylinders of high-purity fused silica, with a core of slightly higher index material. Down the axis, light is guided by the index of refraction gradient of the core and is propagated as a quasi-Gaussian beam with mode radius $w \approx 2$ $\mu$m with an attenuation coefficient of $\leq 14$ dB/km. No higher-order modes are guided, and while one may initially assume that the fiber is free of birefringence, polarization states cannot be clearly separated.[24]

In such a system, the only feasible way to distinguish the pump input and output waves in four-wave mixing is by frequency. Consider a pump wave of frequency $\omega_1$ propagating in the positive $z$ direction with amplitude $E(\omega_1)$. The pump wave couples a copropagating probe wave with frequency and amplitude $\omega_2$ and $E(\omega_2)$ to the complex conjugate of a signal wave of frequency $\omega_3 = 2\omega_1 - \omega_2$ and amplitude $E(\omega_3)$,[25]

$$\frac{\partial E(\omega_3)}{\partial z} = \frac{i3\omega_3}{2nc} f_3 \chi^{(3)} E^2(\omega_1) E^*(\omega_2) - \frac{\alpha}{2} E(\omega_3) , \tag{1}$$

$$\frac{\partial E(\omega_2)}{\partial z} = \frac{i3\omega_2}{2nc} f_2 \chi^{(3)} E^2(\omega_1) E^*(\omega_3) - \frac{\alpha}{2} E(\omega_2) , \tag{2}$$

where

$$\chi^{(3)} = \chi^{(3)}_{1111}(\omega_3, \omega_1, \omega_1, -\omega_2)$$
$$= 0.5 \times 10^{-14} \text{ esu} \approx 0.6 \times 10^{-23} \text{ mks units}$$

is the optical nonlinearity (for constant parallel polarization), and $\alpha \approx 3 \times 10^{-3}$ m$^{-1}$, the attenuation coefficient for silica fibers. Equations (1) and (2) are in mks units; in the more familiar esu system, the first term on the right of the equal sign must be multiplied by a factor of $4\pi$.

The $E(\omega_j)$ are the Fourier amplitudes of the electric field

$$E(\mathbf{r},t) = \tfrac{1}{2} \sum_j E(\omega_j) F_j(x,y) e^{-i\omega_j t} e^{+ik_j z} + \text{c.c.} \tag{3}$$

In Eqs. (1) and (2), the transverse spatial profiles are specified by the dimensionless functions $F_j(x,y)$.[25] The overlap factor

$$f_j = \frac{\int |F_1(x,y)|^2 F_2(x,y) F_3(x,y) dx\, dy}{\int |F_j(x,y)|^2 dx\, dy} \tag{4}$$

has been employed to account for any mismatch in beam profiles. The frequency shift $\varepsilon = \omega_1 - \omega_2$ has been assumed small enough that phase-matching considerations can be neglected.[26] In practice for a 100 m length of fiber, this approximation is justified up to $\varepsilon = \omega_1 - \omega_2 \sim 1$ GHz, in which case $\varepsilon/\omega_i \leq 2 \times 10^{-6}$.

The dimensions of $E$ are V/m in Eqs. (1)—(3) and the intensity has the dimensions W/m$^2$. It is more convenient and customary in quantum optics to express optical field amplitudes in units such that the square of the amplitude is proportional to the number of quanta in the field; such a parametrization requires the definition of a quantization volume.[27] For traveling waves in an optical fiber, it is more useful to define the field in terms of the number of quanta per second passing through the area $A_j = \int |F_j(x,y)|^2 dx\, dy / |F_j(0,0)|^2$ of the confined mode. Since in our experiments all optical frequencies are very near $\omega_j$, the intensity of each frequency component $\omega_j$ is

$$I_j = \frac{nc\epsilon_0}{2} |E(\omega_j)|^2 . \tag{5}$$

The power and the intensity in the guided mode are related by $I_j A_j = P_j$ and the quantization volume is $V_Q = A_j l$, where $l$ is the fiber length.

The pump field can be treated classically, but correct description of squeezed-state generation requires the probe and signal amplitudes to be described by operators

$$\tilde{E}(\omega_2) = \left[ \frac{\hbar\omega}{\epsilon V_Q} \right]^{1/2} a_2 , \tag{6}$$

$$\tilde{E}(\omega_3) = \left[ \frac{\hbar\omega}{\epsilon V_Q} \right]^{1/2} a_3 , \tag{7}$$

where $a_2$ and $a_3$ obey the boson commutation relations

$$[a_i, a_j^\dagger] = \delta_{ij}$$

and $\epsilon = n^2 \epsilon_0$. The quantized equations describing four-wave mixing corresponding to the classical Eqs. (1) and (2) are

$$\frac{d}{dz} a_2 = -i\kappa E^2(\omega_1) a_3^\dagger , \tag{8}$$

$$\frac{d}{dz} a_3^\dagger = i\kappa^* [E^*(\omega_1)]^2 a_2 , \tag{9}$$

where

$$\kappa = \frac{3\omega_1}{2nc} f_2 \langle \chi^{(3)}(-\omega_3, \omega_1, \omega_1 - \omega_2) \rangle$$

is the coupling constant. The average over $\chi^{(3)}$ accounts for the possible effects of varying polarizations within the fiber. Loss has been ignored and $f_2$ has been assumed equal to $f_3$. These operator equations follow from the interaction Hamiltonian

$$\mathcal{H} = \hbar\kappa E^2(\omega_1) a_2^\dagger a_3^\dagger + \text{H.c.} \tag{10}$$

with $z = ct/n$.

The solutions for the operators at the end of the fiber $z = l$ are

$$a_2(l)=a_2(0)\cosh[|\kappa|\,|E(\omega_1)|^2 l] - ia_3^\dagger(0)\frac{\kappa E^2(\omega_1)}{|\kappa|\,|E(\omega_1)|^2}\sinh[|\kappa|\,|E(\omega_1)|^2 l]\ , \tag{11a}$$

$$a_3(l)=a_3(0)\cosh[|\kappa|\,|E(\omega_1)|^2 l] - ia_2^\dagger(0)\frac{\kappa E^2(\omega_1)}{|\kappa|\,|E(\omega_2)|^2}\sinh[|\kappa|\,|E(\omega_j)|^2 l]\ . \tag{11b}$$

The case with finite loss has been treated in Ref. 17.

For the case where the input to the fiber in modes at $\omega_2$ and $\omega_3$ are only vacuum fluctuations, the mean amplitude at the output is

$$\langle \tilde{E}(\omega_j,l)\rangle = 0$$

for $j=2,3$ and the mean-square amplitude

$$\langle |\tilde{E}(\omega_j,l)|^2\rangle = \frac{1}{\epsilon}\frac{\hbar\omega_j}{V_Q}\langle a_j^\dagger a_j\rangle = \frac{\hbar\omega_j}{\epsilon V_Q} \times \sinh^2[|\kappa| l\,|E(\omega_1)|^2] \ll |E(\omega_1,l)|^2\ . \tag{12}$$

The wave emanating from the output end of the fiber at $z=l$ is a superposition of the components at the three frequencies

$$E(z=l)\sim[E(\omega_1)e^{-i\omega_1 t}+E(\omega_2)e^{-i\omega_2 t}+E(\omega_3)e^{-i\omega_3 t}]+\text{c.c.}$$

A unit quantum efficiency detector placed in the output beam from such a fiber would produce an average electric current equal to the electron charge times the average photon flux $I_1/\hbar\omega_1$ due to the pump wave. Fluctuations in the intensity due to beating between the pump wave and the two weaker waves would produce ac detector currents at the beat frequency. The mean square of these ac currents represents a detector noise power which can be measured electrically.[28] The current $i(t)$ produced by a unit quantum efficiency detector due to an instantaneous light intensity $I(t)$ is

$$i(t)=\frac{e}{\hbar\omega}I(t)A\ , \tag{13}$$

where $e$ is the magnitude of the charge on the electron, $A$ is the area of the detector, and $\omega$ is the frequency of the light. It is convenient to resolve the detector current into Fourier components $i(\varepsilon)$ and to relate these components directly to Fourier components of the intensity.

The local oscillator wave (which is derived from the pump wave) reaches the detector with an amplitude that can be treated classically. We define a local oscillator amplitude $E_{\rm LO}$ and introduce a phase $\phi/2$ being the phase difference between the local oscillator and the pump as well as a pump attenuation coefficient $\mathcal{T}$, both defined at the exit plane of the fiber as

$$E_{\rm LO}=\mathcal{T}E(\omega_1)e^{i\phi/2}=E_R e^{i(\theta+\phi/2)}\ . \tag{14}$$

The complex amplitude is written as $\mathcal{T}E(\omega_1)=E_R e^{i\theta}$ where $\theta$ is an absolute phase that may vary slowly in time as the pump phase diffuses, and $E_R$ is real. The dominant contribution to the $\varepsilon\neq 0$ Fourier components of the intensity at the detector result from beating between this classical local-oscillator wave and the frequency-shifted signal and idler waves which are treated quantum mechanically. The appropriate operator is

$$\tilde{I}(\varepsilon)=\frac{nc\epsilon_0}{2}\{E_{\rm LO}^*(\omega_1)[\tilde{E}(\omega_1+\varepsilon)+\tilde{E}(\omega_1-\varepsilon)] + E_{\rm LO}(\omega_1)[\tilde{E}^\dagger(\omega_1+\varepsilon)+\tilde{E}^\dagger(\omega_1-\varepsilon)]\} = \frac{nc\epsilon_0}{2}\left[\frac{\hbar\omega}{\epsilon V_Q}\right]^{1/2}[E_{\rm LO}^*(\omega_1)(a_2+a_3) + E_{\rm LO}(\omega_1)(a_2^\dagger+a_3^\dagger)] \tag{15}$$

and the average detector current at frequency $\varepsilon$ is

$$\langle i(\varepsilon)\rangle=\frac{eA}{\hbar\omega}\langle\tilde{I}(\varepsilon)\rangle\ . \tag{16}$$

In (15) and (16), $\varepsilon$ has been assumed large enough that technical noise on the local oscillator is absent.

Electronic spectrum analyzers measure the power in an electrical signal at frequency $\varepsilon$ within an electronic bandwidth $\Delta\varepsilon$. For a photodetector producing a current $i(t)$, the electronic-power spectral density is

$$N(\varepsilon)=\langle i^2(\varepsilon)\rangle R\ , \tag{17}$$

where $R$ is the electrical resistance. Thus, the quantity measured when optical signals and noise is detected on the spectrum analyzer is

$$N(\varepsilon)=\left[\frac{e}{\hbar\omega}\right]^2 A^2 R\langle I^2(\varepsilon)\rangle\ . \tag{18}$$

It is convenient to define the variance of the Fourier component of the (current and) intensity at frequency $\varepsilon$,

$$V_I(\varepsilon)=\langle I^2(\varepsilon)\rangle-\langle I(\varepsilon)\rangle^2\ . \tag{19}$$

The case of $\varepsilon=0$ where the pump wave beats with itself has been purposely omitted. When $\langle E(\omega_j)\rangle=0$ for $j=2,3$, the quantity experimentally measured, $N(\varepsilon)$, is directly related to $V_I(\varepsilon)$ by

$$N(\varepsilon)=\left[\frac{e}{\hbar\omega}\right]^2 V_I(\varepsilon)A^2 R\ . \tag{20}$$

We shall now show that the experimentally measured quantity $N(\varepsilon)$ describing the electronic fluctuations at frequency $\varepsilon$ is directly related to the quadrature phase amplitudes at modulation frequency $\varepsilon$ by calculating the variance $V_I(\varepsilon,\phi)$ of the detected intensity at the end of the

fiber. We write

$$e=\frac{a_2+a_3}{2}=X_1+iX_2\ . \tag{21}$$

One can define a variance of the field components at phase $\phi/2$ and frequency shift $\varepsilon$ which is analogous to the variance defined previously for the degenerate case:[1,29–31]

$$\begin{aligned}V(\varepsilon,\phi)=&\cos^2(\phi/2+\theta)(\langle X_1^2\rangle-\langle X_1\rangle^2)\\&+\sin^2(\phi/2+\theta)(\langle X_2^2\rangle-\langle X_2\rangle^2)\\&-\sin(\phi+2\theta)\left[\frac{\langle X_1X_2\rangle+\langle X_2X_1\rangle}{2}-\langle X_1\rangle\langle X_2\rangle\right].\end{aligned} \tag{22}$$

The variance of the intensity at the detector is then

$$\begin{aligned}V_I(\varepsilon,\phi)&=\langle I^2(\varepsilon)\rangle-\langle I(\varepsilon)\rangle^2\\&=2\frac{c^2\epsilon_0\hbar\omega}{V_Q}\,|E(\omega_1)|^2V(\varepsilon,\phi)\ ,\end{aligned} \tag{23}$$

or in terms of the local-oscillator intensity,

$$V_I(\varepsilon,\phi)=\frac{4\hbar\omega c}{nV_Q}I_{\rm LO}V(\varepsilon,\phi)\ . \tag{24}$$

The relevant field quadrature variance may also be expanded in terms of $e$, giving

$$\begin{aligned}V(\varepsilon,\phi)=\tfrac{1}{4}+\tfrac{1}{4}[&2\langle e^\dagger e\rangle-2\langle e^\dagger\rangle\langle e\rangle\\&+e^{-i\phi-2i\theta}(\langle e^2\rangle-\langle e\rangle^2)\\&+e^{i\phi+2i\theta}(\langle e^{\dagger 2}\rangle-\langle e^\dagger\rangle^2)]\ .\end{aligned} \tag{25}$$

The spectral density of the noise power is

$$\begin{aligned}N(\varepsilon)d\varepsilon&=\langle i^2(\varepsilon)\rangle R\,d\varepsilon\\&=\left[\frac{eA}{\hbar\omega}\right]^2\left[\frac{4\hbar\omega c}{nV_Q}\right]I_{\rm LO}V(\varepsilon,\phi)R\,d\varepsilon\ ,\end{aligned} \tag{26}$$

where $R$ is the resistance of the detector. Note that for $E(\omega_2)$ and $E(\omega_3)$ in vacuum states, the usual coherent state results are obtained[1,29]

$$\begin{aligned}&V(\varepsilon,\phi)\,|_{\rm coh}=\tfrac{1}{4}\ ,\\&V_I(\varepsilon,\phi)\,|_{\rm coh}=\frac{\hbar\omega c}{nV_Q}I_{\rm LO}\ .\end{aligned} \tag{27}$$

Squeezing occurs when the noise in Eq. (26) is less than

$$N_{\rm coh}=R\frac{e^2cA^2}{nV_Q\hbar\omega}I_{\rm LO}\ . \tag{28}$$

The factor $cA/nV_Q$ represents an intrinsic bandwidth due to the time of propagation down the fiber of volume $V_Q$. The area $A$ is formally that of the detector, but may be assumed equal to the fiber mode. The nonlinear interaction [described by the Hamiltonian (10)] in the fiber alters the variance of the quadrature amplitude operators. We find for the initial state of $a_2$ and $a_3$ in the vacuum

$$\langle e\rangle=\langle e^\dagger\rangle=0=\langle e\rangle^2=\langle e^\dagger\rangle^2\ , \tag{29a}$$

$$\langle e^\dagger e\rangle=\langle a_2^\dagger a_2\rangle=\sinh^2[\,|\kappa|\ |E_1(\omega)|^2l]\ , \tag{29b}$$

$$\begin{aligned}\langle e^2\rangle=\langle a_2a_3\rangle=&-\frac{i\kappa e^{2i\theta}}{|\kappa|}\cosh[\,|\kappa|\ |E_1(\omega)|^2l]\\&\times\sinh[\,|\kappa|\ |E_1(\omega)|^2l]\ ,\end{aligned} \tag{29c}$$

which yields

$$\begin{aligned}V(\varepsilon,\phi)=&\tfrac{1}{4}+\tfrac{1}{2}\sinh^2[\,|\kappa|\ |E(\omega_1)|^2l]\\&+\tfrac{1}{2}\mathrm{Im}\left[e^{-i\phi}\frac{\kappa}{|\kappa|}\right]\cosh[\,|\kappa|\ |E_1(\omega_1)|^2l]\\&\times\sinh[\,|\kappa|\ |E_1(\omega_1)|^2l]\ .\end{aligned} \tag{30}$$

We note that the variance $V(\varepsilon,\phi)$ is independent of the absolute phase $\theta$, and thus insensitive to phase diffusion of the laser source.[32] The nonlinear susceptibility of glass is known to be real and positive at the frequencies of interest.[25] The coupling constant $\kappa$ must then be real and positive for an optical-fiber medium. Hence, the optimally squeezed component is measured if one selects $\phi=\pi/2$.

For $\phi=0$, the noise spectral density is increased and the output of a fiber is more noisy than the coherent-state input. However, if the phase of the local oscillator could be shifted by $\pi/4$ with respect to the transmitted pump (i.e., $\phi=\pi/2$), the detector-noise spectral density would fall below that of $N_{\rm coh}(\varepsilon)$ and thus squeezing would be demonstrated. Such a phase shift can be accomplished by a variety of interferometric techniques, one of which will be described in Sec. IV.

## III. ANHARMONIC-OSCILLATOR MODEL FOR AN OPTICAL FIBER

The calculation of the preceding section treats the nonlinear susceptibility of an optical fiber as a classical quantity. Previous publications have shown, however, that such a treatment is an approximation at best, and that the true quantum nature of $\chi^{(3)}$ can produce additional noise.[18] It is thus instructive to parametrize the linear and nonlinear optical properties of silica-glass optical fibers in terms of some solvable quantum model and to see the extent to which a classical approximation applies. A quantum model also facilitates correct treatment of fiber attenuation. The quantum model chosen was the anharmonic-oscillator treatment of Reid and Walls.[33] The relevant optical parameters of glass fiber are the index of refraction $n=1.45$, the atomic absorption constant $\alpha=3\times10^{-3}$ m$^{-1}$, the effective nonlinear susceptibility $6\chi^{(3)}=3\times10^{-14}$ cm$^3$/erg$\approx4\times10^{-23}$ mks. The laser frequency $\omega\sim3\times10^{15}$ sec$^{-1}$ was assumed to lie far below any transition from the ground state. The anharmonic-

oscillator analysis requires assignment of model values of the glass. The Classius-Mossotti equation for the complex index of refraction

$$\frac{n^2-1}{n^2+1}=\frac{\chi}{3} \tag{31}$$

relates $n=n_R+in_I$ to the complex susceptibility of the medium $\chi=\chi'+i\chi''$ (in mks units). Since $n_R \gg n_I$ and $\chi' \gg \chi''$, Eq. (31) can be directly applied to yield $\chi'$. The imaginary part of the susceptibility $\chi''$ can be related to fiber attenuation constant $\alpha$ by expanding Eq. (31) and keeping the first nonvanishing imaginary terms

$$\alpha=2n_I\frac{\omega}{c}=\left[\frac{n_R^2+2}{3}\right]^2\frac{\omega}{2n_Rc}\chi'' . \tag{32}$$

For typical fibers with $n_R=1.45$ and $\alpha=3\times10^{-3}$ m, these formulas yield $\chi'=0.81$ and $\chi''=4\times10^{-11}$.

The Hamiltonian for the anharmonic-oscillator model considered for the medium by Reid and Walls[33] is given by

$$\begin{aligned}\mathscr{H}=&\hbar\Omega b^\dagger b+\hbar W(b^\dagger)^2b^2\\&+\hbar g\sum_{j=1}^{3}[b^\dagger\tilde{E}(\omega_j)e^{-i\omega_jt}+b\tilde{E}^\dagger(\omega_j)e^{i\omega_jt}]\\&+b\Gamma_R^\dagger+b^\dagger\Gamma_R ,\end{aligned} \tag{33}$$

where $\Omega$ is the oscillator frequency, $b$ is the oscillator operator, and $E(\omega_1)$ is the pump field. The weak sideband fields are represented by $\tilde{E}(\omega_2)$ and $\tilde{E}(\omega_3)$ as defined in Eqs. (6) and (7). The field-oscillator coupling is specified by the parameter

$$g=\left[\frac{\omega_1}{\hbar V_Q}\right]^{1/2}\mu , \tag{34}$$

where $\mu$ is the dipole-moment operator and $V_Q$ is the quantization volume. The reservoir operators $\Gamma_R$ and $\Gamma_R^\dagger$ give rise to a loss rate $\Gamma$. The nonlinearity parameter $W$ is responsible for the interaction that gives rise to squeezing. The work of Reid and Walls[18,21,33] shows the squeezing in the output field to be a function of two scaled parameters, namely, the scaled detuning $\delta=(\Omega-\omega_1)/\Gamma$ and the scaled medium intensity $|\beta_0|^2$. In the perturbative regime (satisfying $|\delta| \gg |\beta_0|^2$), $|\beta_0|^2$ is related to the driving field intensity as follows:

$$|\beta_0|^2=\frac{Wg^2}{\delta^2\Gamma^3}|E(\omega_1)|^2 . \tag{35}$$

In order to calculate the values of $\delta$ and $|\beta_0|^2$ corresponding to the experiment, we fit the model to the appropriate $\chi^{(3)}$ values for the glass fiber. The equations for four-wave mixing in a medium modeled by anharmonic oscillators are derived in Ref. 33. After elimination of the oscillator variables, the following equation is obtained for the $c$-number stochastic field amplitudes $\alpha_j=\langle\tilde{a}_j\rangle$ of the weak fields ($j=2,3$):

$$\alpha_j=-igP_j , \tag{36}$$

where $P_j$ is the medium polarization which may be expanded in the perturbative regime as

$$P_j=\epsilon_0\left[(\chi'+i\chi'')\alpha_j+6\left[\frac{3}{n^2+2}\right]^4 f_2\chi^{(3)}|E(\omega_1)|^2\alpha_{5-j}^*+F_j(t)\right] , \tag{37}$$

where the factor of 6 in the second term results from permutation symmetry, and mks units have been assumed.[34]

Reservoir fluctuations are represented by the fluctuating force $F_j(t)$. The anharmonic-oscillator model of Reid and Walls[33] gives

$$\dot{\alpha}_j=-(\gamma_R+i\gamma_I)\alpha_j-i\,\mathfrak{X}\,\alpha_{5-j}^*+\Gamma(t) , \tag{38}$$

where $\Gamma(t)$ is a fluctuating force. In the perturbative regime,

$$\begin{aligned}\gamma_R&=\frac{2C}{1+\delta^2}\equiv\epsilon_0g\chi'' ,\\ \gamma_I&=\frac{2C\delta}{1+\delta^2}\equiv\epsilon_0g\chi' ,\\ |\mathfrak{X}|&=\frac{4C}{1+\delta^2}|\beta_0|^2=6\epsilon_0\left[\frac{n^2+2}{3}\right]^{-4}f_2|\chi^{(3)}||E(\omega_1)|^2 ,\end{aligned} \tag{39}$$

and $2C=\epsilon_0g^2N/\Gamma$, where $N$ is the number of oscillators. The phases have been set to correspond to the fiber case. The nonlinear optical susceptibility of the medium is contained in the parameter $\mathfrak{X}$ which has been defined to incorporate the local field correction effects.[13]

Immediately, we see the scaled detuning is simply the ratio of $\chi'$ to $\chi''$,

$$\delta=\frac{\gamma_I}{\gamma_R}=\frac{\chi'}{\chi''}\approx2\times10^{10} . \tag{40}$$

In fact, the anharmonic-oscillator model predicts that for $\delta>10$, the only factor destroying squeezing is the loss parameter $\gamma_R$, i.e., the ratio of loss to coupling ($\gamma_R/|\mathfrak{X}|$) must be small for good squeezing. This ratio is in fact related to the intensity parameter $|\beta_0|^2$. Examination of Eq. (39) shows

$$\begin{aligned}|\beta_0|^2=\frac{|\mathfrak{X}|}{2\gamma_R}&=\frac{3(n^2+2)^{-4}|\chi^{(3)}|\,|E(\omega_1)|^2}{\chi''}\\&=\left[\frac{n^2+2}{3}\right]^{-6}\frac{2\kappa|E(\omega_1)|^2}{\alpha} ,\end{aligned} \tag{41}$$

where the last equation expresses $(\beta_0)^2$ in the same terms as Eqs. (1)–(30), with constant polarization.

A 100 m length of fiber with a 2 $\mu$m radius core has quantization volume $V_Q=1.2\times10^{-3}$ cm$^3=1.2\times10^{-9}$ m$^3$. With 1 W of laser power in that core, the intensity is 80 GW/m$^2$, which implies $|E(\omega_1)|^2=2.3\times10^4$ erg/cm$^3=2\times10^{13}$ V$^2$/m$^2$. Thus, $|\beta_0|^2$ is of the order of 3. Clearly, the perturbative condition ($\delta \gg |\beta_0|^2$) assumed above is satisfied.

One might object that many aspects of this model are naive. For example, one might anticipate that phonon

broadening and other effects should increase the homogeneous linewidth of a room-temperature fiber beyond the value given in Eq. (39); however, the fact that the phonon spectrum is bounded by a frequency many times less than the detuning $\Omega-\omega$ implies that phonons can have no effect on the far-wing absorption. In the anharmonic-oscillator model, those wings are correctly described as due only to radiative effects which are not bounded in frequency. The values we obtain for $\Gamma$ and $\delta$ are consistent with radiative damping. The parametrization above is admittedly grossly oversimplified and somewhat pessimistic. The actual attenuation, e.g., in an optical fiber is due mostly to light scattering and not due to absorption by the transitions responsible for the index of refraction. Even so, one can employ this model to estimate the additional noise produced by the quantum nature of the medium under the conditions of our proposed experiment.

The appropriate phase-matched equations for the weak fields are derivable directly from Eq. (38). These have been solved by Reid and Walls[33] and the variance $V(\epsilon,\phi)$ derived as a function of $|\beta_0|^2$ for the scaled detuning $\delta$ given above is plotted in Fig. 1. The curves are insensitive to the precise value of $\delta$, provided $\delta>10$. At lower intensities ($|\beta_0|^2<1$), attenuation of the medium dominates and minimizes the squeezing otherwise possible due to the nonlinear coupling. At high pumping powers, the quantum anharmonic oscillator does not contribute excess noise to the optical fields, even in the presence of moderate absorption. Thus, one might imagine that the model of Kumar and Shapiro[17] which treated the loss and medium in a phenomenological manner is validated by this result. In particular, the length of the fiber does not affect the squeezing for $\alpha l<1$ and $|\beta_0|^2>1$.

However, the absence of noise contributed by the quantum-mechanical medium may result from the choice of an anharmonic-oscillator model to describe the medium. Other models[18,21]—particularly the two-level atom model—are known to predict excess noise at high pump powers and thus lead to reduced squeezing, especially at moderate values of the detuning $\delta$. We also attempted to fit the optical-fiber nonlinearity to a two-level atom model, and generally succeeded except that the sign of the optical nonlinearity was incorrect. In a two-level atom away from resonance, nonlinear effects must act to reduce the magnitude of the total susceptibility. Since the linear susceptibility is positive ($n>1$) below resonance, the nonlinear susceptibility must be negative.

General considerations, similar to those used here to fit the fiber data to the anharmonic-oscillator model, resulted in a reasonable parametrization of a model two-level atom medium with a nonlinearity having the correct magnitude. The methods of Reid and Walls[18,21] then showed that even that medium would produce squeezing consistent with that predicted for the anharmonic-oscillator model at the power levels accessible in our apparatus. The excess noise resulting from population of the excited state was insignificant since the detuning $\delta$ from resonance was so great that sufficient nonlinear interaction took place with negligible population transfer. The fact that two quantum models that differ so greatly in their details predict squeezing comparable to the Kumar-Shapiro model[17]

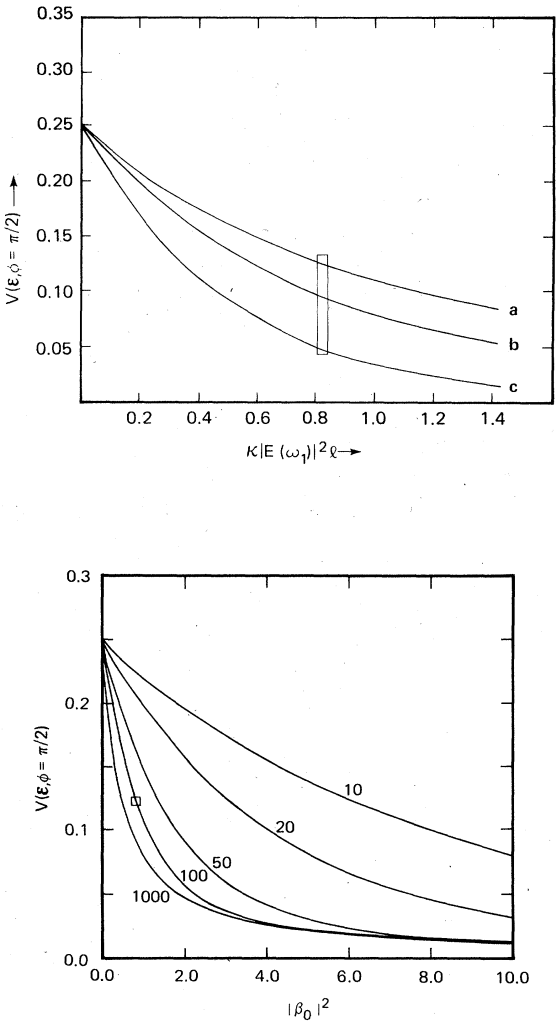


FIG. 1. (a) Field quadrature variance as defined in Eq. (25) as a function of the nonlinear coupling. Curve $a$ is the result of the anharmonic-oscillator model $l=100$ m and $\alpha=3\times10^{-3}$ m$^{-1}$. In that case $|\beta_0|^2=\kappa|E(\omega_1)|^2 l$. Curve $b$ is an anharmonic-oscillator result for $l=100$ m and $\alpha=1\times10^{-3}$ m$^{-1}$. This case corresponds approximately to a length of fiber with 0.5-dB loss or $\alpha l=0.12$ as described in the text. The value of $|\beta_0|^2$ is $3.3\kappa|E(\omega_1)|^2 l$ for this curve. Pump attenuation and depletion have been neglected. Curve $c$ shows the semiclassical results of Eq. (30) in which loss has been ignored. All three curves are consistent with the semiclassical theory of Ref. 17. The box indicates the region expected to be accessible in our experiment in which the stimulated Brillouin effect limits the pump power. (b) Field quadrature variance as a function of normalized pump power for the fiber with $\alpha=3\times10^{-3}$ m$^{-1}$. The numbers labeling the curves indicate the total fiber length in meters. The attenuation of the weak waves in this geometry does not disastrously decrease squeezing so long as pump depletion can be neglected. When the nonlinear interaction exceeds the attenuation and $\alpha l\lesssim 1$, increasing the fiber length improves the squeezing. The result for infinite fiber length agrees with that for 1000 m to the accuracy of this plot. While the anharmonic-oscillator model has produced these data, these plots are also consistent with the theory of Ref. 17. The two-level atom model would differ for long fibers.

under the conditions of our fiber experiment suggests that such an experiment has a considerable chance of success.

## IV. PROPOSED EXPERIMENT

The foregoing discussion implies that squeezed states can be generated by nondegenerate four-wave mixing in an optical fiber. For an unequivocal demonstration, the noise spectral density of Eq. (20) must be reduced by a factor of 10 below that of a coherent state Eq. (28). Such a reduction requires that the fiber length $l$, pump amplitude $E(\omega_1)$, and effective nonlinearity $\kappa$ fulfill

$$|\kappa|\,|E(\omega_1)|^2 l > \tfrac{1}{2}\ln 10 \approx 1.15\ , \tag{42}$$

where the attenuation constant has been temporarily set to zero. To detect the squeezed state generated in an optical fiber, one must also phase shift the pump wave at frequency $\omega_1$ by $\pm\pi/4$ to produce a local oscillator wave at the detector which beats with the squeezed quadrature. Such a phase shift can be conveniently imposed by a confocal Fabry-Perot resonator used in reflection.[35,36]

Consider the off-axis confocal resonator diagrammed in Fig. 2. The input mirror has an intensity reflection coefficient $\rho$ and transmission $T$. The back mirror of the cavity has reflectivity $\rho'$ and transmission $T'$ where $T \gg T'$ and $\xi = 1-\rho \gg 1-\rho' = \eta$. A wave of complex amplitude $E_I(\omega)$ is incident upon this device. The reflected amplitude $E_R$ and transmitted amplitude $E_T$ are given by

$$E_R = -\sqrt{\rho}\left[1-\frac{\rho' T e^{i\Delta}}{1-\rho\rho' e^{i\Delta}}\right]E_I$$

$$\approx \left[\frac{\Delta^2+\eta(\eta+\xi)-i\xi\Delta}{\Delta^2+(\eta+\xi)^2}\right]E_I\ , \tag{43}$$

$$E_T = \frac{T(\rho')^{1/2}E_I}{1-\rho\rho' e^{i\Delta}} \approx T\sqrt{\xi}\left[\frac{\Delta^2/2+(\xi+\eta)+i\Delta}{\Delta^2+(\xi+\eta)^2}\right]E_I\ , \tag{44}$$

where $\Delta = (n\omega/c)l_c - \Delta_j$ is the detuning of the incident frequency from the $j$th transmission resonance, $l_c$ is the optical length of the cavity, $\Delta_j$ accounts for any phase shift due to reflection at the mirrors, and $\Delta_{j+1} = \Delta_j + 2\pi$. Resonances occur at $\Delta \approx 0$ and the approximate expressions are appropriate for $|\Delta| \ll 1$. Near a transmission resonance, the amplitude and phase of reflected wave $E_R$ are given by

$$|E_R|^2 = |E_I|^2\left[\frac{\Delta^2+\eta^2}{\Delta^2+(\eta+\xi)^2}\right]\ , \tag{45}$$

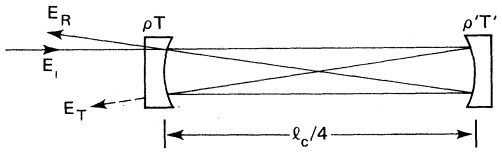


FIG. 2. Reflective Fabry-Perot interferometer cavity as used to provide a local-oscillator wave. The mirror reflectivities are $\rho$ and $\rho'$, while the transmission coefficients are $T$ and $T'$. The incident, reflected, and transmitted field amplitudes are indicated along the corresponding propagation directions.

$$\Phi_R = \tan^{-1}\left[\frac{-\xi\Delta}{\Delta^2+\eta(\eta+\xi)}\right]\ . \tag{46}$$

The maximum phase shift possible on a single reflection from such a cavity is

$$\Phi_{\max} = \tan^{-1}\left[\frac{1}{2}\left[\frac{\xi}{\eta}\right]^{1/2}\right] \tag{47}$$

which occurs at detuning $\Delta_{\max} = \sqrt{\eta(\eta+\xi)}$.

In a realistic cavity $T \approx 10T'$, implying a maximum phase shift of $\sim\pi/3$. To achieve a $\pi/2$ phase shift, one must reflect the beam $E_R$ back onto the cavity to double the effect. The reflected wave with phase shift $2\Phi$ then becomes the local oscillator wave at the detector. The use of a Fabry-Perot resonator to shift phases in this way also reduces the intensity of the local oscillator to a level that can be withstood by a $p$-$i$-$n$ photodiode.

Returning to the single-reflection geometry, one can define a phase shift between a carrier wave near a cavity resonance and sidebands detuned from resonance as

$$\phi/2 = \Phi_R(\omega_1) - [\Phi_R(\omega_2)+\Phi_R(\omega_3)]/2\ . \tag{48}$$

In Eq. (48), the phase shift $\phi/2$ has the same meaning as $\phi/2$ in Eq. (14), while the phases $\Phi(\omega_j)$ correspond to Eq. (46) with $\Delta = (n\omega_j/c)l_c - \Delta_k$. The carrier wave at $\omega_1$ is closer to resonance than the other frequency components and thus experiences most of the phase shift. Frequency components shifted from the pump by frequency $\varepsilon \gg (\eta+\xi)c/nl_c$ are not phase shifted by the cavity. For such frequency components, the cavity can be regarded as a simple mirror with reflection coefficient $\rho$. Squeezing is not adversely affected if $\rho > 1-4V(\varepsilon,\phi)$.

In our proposed experiment, a pump wave of power $P(\omega_1)$ is focused into a fiber of length $l$ as shown in Fig. 3. The pump wave is produced by a single-mode krypton ion laser oscillating at 647 nm and isolated from fiber reflections by a Faraday rotator. The pump frequency is $\omega_1$, stabilized electronically, and the inputs to the fiber at frequencies $\omega_2$ and $\omega_3$ are merely vacuum fluctuations.

The four-wave mixing effect in the fiber causes squeezing at the output. The transmitted waves are reflected from a confocal cavity as described above. The cavity resonant frequency is locked at a constant offset to the pump frequency to provide the required phase shift. The beam reflected from the cavity is detected by a high-speed silicon $p$-$i$-$n$ photodiode $D$ with quantum efficiency above 83%. The optical power level at the diode must be sufficient to overcome thermal noise, and the diode output must be amplified by a low-noise circuit. Finally, the power spectrum of the amplified diode output is Fourier analyzed and displayed on an electronic spectrum analyzer. The dc current produced by the photodiode must also be measured to determine the detected power level. The coherent-state quantum noise level at frequency shift $\varepsilon$ is determined by measuring the noise spectral density from the detection system at various dc currents when the laser beam or a powerful incoherent source is incident on the detector.

The signatures of a squeezed state would be (1) a noise level measured at the spectrum analyzer below that ex-

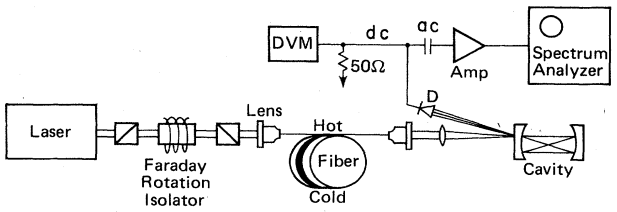


FIG. 3. Overall scheme of the squeezing experiment. Pump power from the stabilized laser is coupled into the fiber which must be subjected to a temperature gradient to suppress the stimulated Brillouin effect. The fiber output is recollimated and coupled into an optical cavity which attenuates and phase shifts the pump light. The local oscillator and sidebands beat at the photodetector $D$, and the electronic noise spectrum and average detector current are recorded.

pected for a coherent state producing the same dc current at the detector, and (2) a noise level that varies with the local oscillator phase as predicted by Eqs. (26) and (30) yielding a noise level below that of a coherent state for $\phi=\pi/2$, and above for $\phi=-\pi/2$.

There are several experimental difficulties to be overcome before squeezed states can be demonstrated in this fashion. Achieving sufficient pump intensity $I(\omega_1)$ in the core of a fiber is the first difficulty. We have found it possible to couple 40% of the laser power into a single-mode core. Since the maximum power of a suitably stable laser is only 3 W, one must choose a fiber capable of reaching the condition of Eq. (42) with $<1$ W of pump power. While the nonlinear susceptibilities of all fused silica fibers are approximately equal and equal to the nonlinear susceptibility of fused quartz ($\chi^{(3)}_{1111}=0.5\times10^{-14}$, $\chi^{(3)}_{1221}=0.2\times10^{-14}$ esu), the intensity obtainable in the core depends on the overlap function $f_2$ and the area of the propagating mode. Thus, the mixing efficiency per unit length varies approximately inversely as the square of the propagating mode radius. Fibers are available with mode radii varying from 1 to 3.5 $\mu$m. Polarization preserving fibers show larger nonlinearities because the larger nonlinear susceptibility $\chi^{(3)}_{1111}$ may always be excited by the linearly polarized waves in such a fiber, whereas random pump polarization couples to an average of the $\chi^{(3)}$ tensor in more common fibers.[24,37] We have performed an extensive series of experiments to determine the best available fiber. These experiments and their results are described in Sec. V. It suffices to say here that the condition of Eq. (42) can be fulfilled in fibers with mode radius $<2$ $\mu$m with $\sim0.5$ W of pump power and $l\sim100$ m.

A more serious limitation results from the physics of narrow-band wave propagation through an optical fiber. Above a certain threshold power, the stimulated Brillouin effect couples the forward-propagating pump wave to a frequency-shifted backward-propagating wave. This stimulated Brillouin reflection clamps the average forward-propagating power at a value near the threshold, which for 100 m of 2 $\mu$m core fiber is typically near 75 mW, well below the power required for squeezing.[38]

The stimulated Brillouin effect has been extensively reviewed.[39] The equation for the amplitude of the backward-propagating wave is

$$-\frac{\partial E_-}{\partial z}=gE_-+\frac{\alpha}{2}E_- , \tag{49}$$

where

$$g(\omega_-)=\frac{g_0\Gamma_B P(\omega_1)}{(\omega_1-\omega_--\Omega_B)^2+\Gamma_B^2} \tag{50}$$

is the Brillouin gain coefficient,

$$\Omega_B=\frac{2\omega_1}{c/nV_s+1}$$

is the frequency shift, $V_s$ is the sound velocity, and $\Gamma_B$ is the homogeneous linewidth of the Brillouin transition.[39] For the traveling-wave case, the threshold for unacceptable attenuation of the forward-propagating pump and unacceptable Brillouin induced noise occurs when

$$g(\omega_-)l\sim5 . \tag{51}$$

This threshold can be suppressed substantially by broadening the Brillouin line shape. The frequency shift $\Omega_B$ depends on the sound velocity, which is somewhat temperature dependent,[40] i.e.,

$$V_s=V_0(1+bT) , \tag{52}$$

where for silica $V_0=5968$ m/s and $b=\sim1\times10^{-4}\,^{\circ}\mathrm{C}^{-1}$.

A sinusoidal temperature distribution of magnitude $\tau$ imposed on the fiber has the effect of broadening the gain curve of Eq. (50), while retaining constant area

$$g(\omega_-)=\frac{g_0\Gamma_B P(\omega_1)}{2\pi}\times\int_0^{2\pi}\frac{d\Theta}{[\omega_1-\omega_--\Omega_B(1+b\tau\sin\Theta)]^2+\Gamma_B^2} . \tag{53}$$

This has the effect of lowering the maximum Brillouin gain and increasing the threshold. Figure 4 shows the transmitted and reflected power as a function of the input power for a 100 m length of 4-$\mu$m-core-diameter fiber with and without a 200° temperature gradient. The Brillouin threshold can be raised to more than 250 mW by

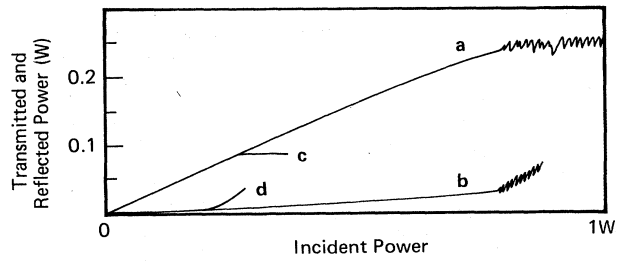


FIG. 4. Suppression of stimulated Brillouin scattering by an imposed temperature gradient. Curves $a$ and $b$ show the transmitted and reflected power, respectively, from a fiber subjected to a 200° temperature gradient. Curves $c$ and $d$ show the transmitted and reflected power from the same fiber at room temperature. The temperature gradient lowers the SBS gain and raises the threshold, making possible larger pump transmission.

this technique. In practice, the 10-cm-diam coil of fiber is heated at the top and cooled by cold nitrogen gas boiled from liquid nitrogen at the bottom.

A second—and unexpected—acoustic effect produces phase modulation of the transmitted probe light. Thermally excited transverse modes of the fiber structure cause compression, dilatation, and uniaxial stress at the core of the fiber, thus modulating the transmitted beam.[41] This guided acoustic-wave Brillouin scattering (GAWBS) has been the subject of other articles and a typical spectrum is partially reproduced in Fig. 5.[42] The maxima of the vibrational modes appear at definite frequency shifts $\varepsilon_{Gi}$, and exceed the quantum noise level of Eq. (28) by tens of dB. One might hope that the noise level in the gaps between modes would be equal to the quantum limit, but the minimum noise level depends crucially on the fiber structure.

We have found that the linewidths of the modes depend on the material used for the protective jacket around the silica fiber. Without such a jacket, the damping of the GAWBS modes is very small, but the fibers are unacceptably delicate. Both very soft jacket materials such as silicone rubber and very hard materials such as aluminum give reduced linewidths.

The maximum frequency shift $\varepsilon$ is limited by the frequency response of high-quantum-efficiency photodiodes more than by phase matching or group-velocity matching considerations in a fiber.[25,26] For the FND-100 photodiode produced by EG&G corporation, the maximum useable frequency is $\varepsilon \sim 300$ MHz, well below the frequency shift where fiber properties become significant. The minimum useable frequency shift is set by the width of the transmission resonance of the Fabry-Perot cavity. Within such a resonance, vacuum fluctuations are transmitted through the cavity into the detector. For our initial cavity, the lowest useable frequency shift was 15 MHz.

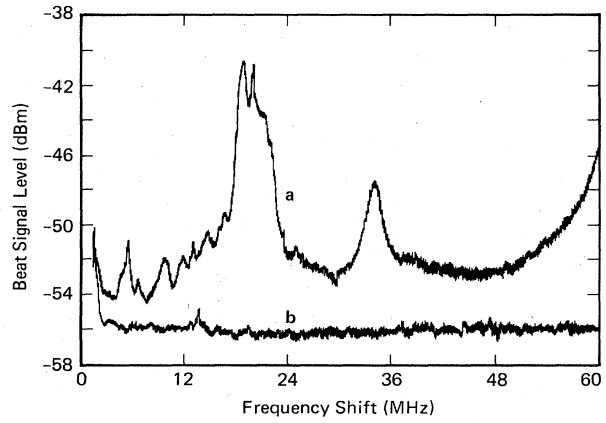


FIG. 5. A portion of the guided acoustic-wave Brillouin scattering (GAWBS) spectrum of 100 m of Hitachi SP-6315 fiber. Trace *a* shows the GAWBS signals for 2-ma photodiode current with 50 mW of pump light transmitted through the fiber. Curve *b* shows the shot plus thermal noise level produced by an incandescent light or laser beam giving the same detector current. The 2-dB increase in the minimum noise level represents phase noise produced by thermally excited mechanical eigenmodes of the fiber. Trace *a* was taken, using the polarization spectroscopy technique of Ref. 42 and corresponds roughly to a 45° phase shift of the local oscillator. The apparatus of Fig. 3 yields similar results except for an additional peak at 29 MHz.

Inside the resonant cavity, the pump wave that has been transmitted through the fiber builds up because of the cavity resonance and can reach an intensity level which damages high-quality cavity mirrors. Thus, one must choose mirrors which can withstand the required power levels as well as provide sufficient phase shift and pump attenuation. Since the reproducibility of the manufacture of such mirrors is not yet assured, selecting a suitable pair of cavity mirrors can be an important subsidiary problem.

Finally, it is essential that the cavity resonance frequency be detuned a correct and stable amount from the laser frequency. This requires careful design of servo electronics for the laser frequency and for the cavity resonance. The cavity phase of Eq. (47) varies more rapidly with the detuning $\Delta$ than does the transmitted and reflected intensity. Fortunately, cavity-locking technology is now a highly developed art, and sufficient stability should be achievable.[44]

Loss due to reflection at optical and detector surfaces and due to scattering in the fiber ultimately limits the degree of squeezing obtained. Antireflection coating can reduce this effect, but a certain number of optical surfaces must be traversed between the fiber and detector. Special coatings may be required to keep the total loss from such effects below 10% or so. Coating the detector surface may also increase the quantum efficiency. While a change from the presently available 83% to 93% in quantum efficiency results in only a 12% increase in signal, it produces more than a factor of 2 increase in detectable squeezing and thus might be a worthwhile goal for those concerned with photodiode development, especially should a squeezed state be experimentally demonstrated.

## V. PRELIMINARY EXPERIMENTS

### A. Fiber characterization

Numerous manufacturers now supply single-mode optical fiber suitable for 647-nm radiation. The nominal specifications vary dramatically from one manufacturer to another, and the actual fiber properties often diverge wildly from specifications. Selection of a fiber suitable for squeezed-states experiments therefore required detailed characterizations of the fibers actually available for purchase. The length of fiber used in an actual experiment must be sufficient to give a decent nonlinear interaction, but not so long as to attenuate the pump or otherwise degrade squeezing. For the purpose of fiber characterization, we have arbitrarily focused on fiber lengths giving 0.5-dB attenuation. When the squeezing is small, the loss due to 0.5-dB fiber attenuation is roughly as important as the imperfect quantum efficiency of our detectors as a limitation on the degree of squeezing. Three simple parameters were of major importance: the attenuation (which varied from 14 to 110 dB/km), the stimulated Brillouin threshold for a length of fiber with 0.5-dB attenuation, and a coefficient

$$K^2=\frac{P(\omega_3, z=0.12/\alpha)}{P(\omega_2, z=0)P^2(\omega_1, z=0)}$$
$$\approx\frac{e^{-3\alpha l}}{(e^{-\alpha l/2}-e^{-3l/2})^2}\frac{P(\omega_3, z=l)1.05\times10^{-2}}{P(\omega_2, z=l)P^2(\omega_1, z=l)} \quad (54)$$

which relates the 4WM signal power to the pump and probe input powers for the 0.5-dB loss fiber (i.e., $\alpha l=0.12$). The second equal sign relates $K$ to measurements made in a fiber with actual length $l$ different from the nominal optimum.

An acceptable fiber would have $KP(\omega_1, z=0)\geq 1$ at a pump power equal to the stimulated-Brillouin-scattering (SBS) threshold. In practice, reaching that criterion requires creating a large temperature gradient along the fiber as discussed previously, and thus it is also important that the fiber tolerate temperature stress. Finally, some region in the GAWBS spectrum must show a noise level near the quantum limit if squeezing is to be detected. GAWBS spectra of all candidate fibers therefore had to be taken at pump power levels comparable to those needed for squeezing.

The manufacturer's attenuation measurements were verified by comparing the power transmitted by a 10 or 100 m length of fiber (depending upon availability) with the transmission of a 0.1 m length. Care was taken to eliminate cladding modes, and to use identical input couplings. The manufacturer's measurements were found to be generally accurate for unstressed fiber. The temperature gradient required to raise the SBS threshold also raised the attenuation in many fibers. We surmised that microbending of the fiber due to contraction of the jacket at low (near liquid nitrogen) temperatures, and due to carbonization at high temperatures was to blame. High and low temperatures will ultimately degrade the performance of any fiber, but those showing increased attenuation at either +200 °C or −100 °C were rejected.

The SBS threshold was measured on 10 or 100 m fiber lengths in an apparatus similar to Fig. 3. The incident, transmitted and reflected powers were measured by three photodiodes and plotted as in Fig. 4. The threshold power was determined as the transmitted power at which the reflection began a more than linear increase. This point also corresponds to the onset of noise bursts in the transmitted radiation and to the appearance of a new spectral component in the reflected beam.

Since no attempt was made to suppress reflections from the ends of the fiber, the SBS threshold measured in this way corresponds to the condition

$$[g(\omega_-)-2\alpha]l+2\ln R=0\,, \quad (55)$$

where $g(\omega_-)$ is the SBS gain in Eq. (53), $\alpha$ is the attenuation constant of the fiber, $l$ is the fiber length, and $R=0.042$ is the reflection coefficient at the ends of the fiber. The factors of 2 appear because SBS light is amplified by interaction with the pump only when traveling in the backward direction, but must make a complete round trip through the fiber (backward and forward) for feedback to occur.[38,39] Estimates of the SBS gain coefficient and threshold for a fiber of length different from $l$ are accurate only to ±30%. Table I summarizes the results of room-temperature measurements. The SBS gain correlates inversely with the area of propagating mode in the fiber core, pretty much as expected. Also shown are the minimum SBS gains obtained using temperature gradients

TABLE I. Characteristics of available single-mode fibers.

| Fiber | Core diameter ($\mu$m) | Attenuation $\alpha$ ($10^3$ m$^{-1}$) | Sample length $l$ (m) | SBS gain 25 °C (m$^{-1}$/W) | SBS gain $\Delta T_{opt}$ (m$^{-1}$/W) | $M$ (dB) | $K$ (W$^{-1}$) |
|---|---|---|---|---|---|---|---|
| Hitachi SP-6315 | 4 | 3.5 | 10.6 | 2.4 | 0.26[a] | 21±1 | 1.2±2 |
| York LB-600 | 3.5 | 3.2 | 7.76 | <1.9 | | 24±1 | 1.6±0.2 |
| BTL 140 | 6.5 | 3.3 | 120 | 0.75 | | 20.3±1 | 1.1±0.2 |
| Newport FSV (1982) | 7 | 2.3 | 11 | 1.2 | | 14.7±1 | 0.56±0.1 |
| Andrew | 1.2 | 24 | 9.8 | 20 | 7.7 | 24±2 | 1.6±0.4 |
| Hughes LTI | 7 | 8.6 | 10.6 | <2 | | 5±1 | 0.20±0.05 |

[a]100 m fiber length.

on two fibers that appeared promising. The large improvement for the Hitachi fiber is consistent with theory; high pump power and/or temperature gradients seemed to cause permanent damage to the Andrew fiber.

To measure the nonlinear mixing coefficient $K$ of these fibers, the apparatus shown in Fig. 6 was assembled. An acousto-optic modulator driven at $\varepsilon_1=71$ MHz provided a pump beam which was focused into the fiber along with a probe beam shifted by $\varepsilon_2=40$ MHz. Four-wave mixing in the fiber produced outputs frequency shifted from the pump by $\pm 31$ MHz. A local-oscillator wave at the laser frequency mixed with the fiber output on the face of a photodiode. The local oscillator was shifted from the pump by $-40$ MHz, thus the nonlinear optical effect in the fiber produce photodiode signals at 102 and 9 MHz. An electronic spectrum analyzer can easily display the levels of these signals along with the 31, 40, and 71 MHz signals due to the beating of the input waves with each other and with the local oscillator.

The beat signal levels at the detector were proportional to the product of the powers of the two waves beating at that frequency. Thus, the power of any optical component can be easily inferred from measurements of a few transmitted power levels and the spectrum-analyzer output.

In the experiment, the pump and probe power transmitted through the fiber was increased from 4 and 2 mW, respectively, to 50 and 35 mW, while the power at the photodiode was held constant with a variable attenuator. The local-oscillator power also remained constant. Under these circumstances, the beats due to the incident frequencies and any nonlinear effects in the photodiode remain constant, while the signals due to the nonlinear effects in the fiber vary as $P^2(\omega_1)P(\omega_2)$. Typical data appears in Fig. 7. We found that with 6 mW of pump light, 7 mW of probe, and 13 mW of local oscillator, the nonlinear signals produced by 10 m of 4-$\mu$m core fiber were 12 dB above the background signals due to detector nonlinearities, etc.

A figure of merit for nonlinear mixing in a fiber can be defined by subtracting one incident beat level (in dB) from the nonlinear signal levels produced by a fiber with length

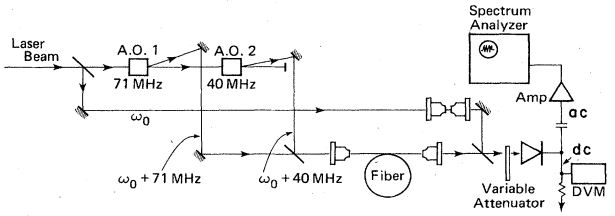


FIG. 6. Apparatus for measuring the optical nonlinearity of a fiber by heterodyne-detected four-wave mixing. The two acousto-optic modulators labeled A.O.1 and A.O.2 produce waves which mix in the fiber by a CARS-like 4WM process (CARS is coherent anti-Stokes Raman spectroscopy). The local-oscillator wave at the laser frequency beats with the amplitudes of the nonlinearly produced waves to give signals on the spectrum analyzer. The laser power can be varied while the diode current is maintained constant with the variable attenuator to verify that the detected signals scale properly with the power in the fiber.

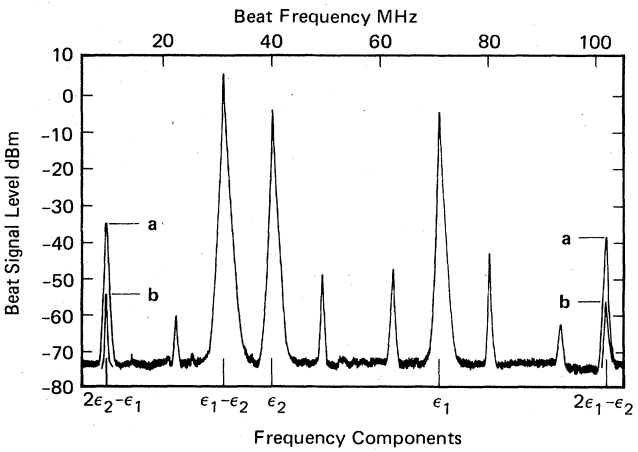


FIG. 7. Spectrum-analyzer output produced by the apparatus of Fig. 5. The frequency shifts of the inputs, their difference, and the outputs are labeled. The fiber is a 10.6 m length of Hitachi SP-6315, and two traces are shown. Trace $a$ corresponds to 50 mW of light frequency shifted by 40 MHz and 60 mW shifted by 71 MHz. Trace $b$ corresponds to 4.5 and 13 mW, respectively. The two traces are almost identical except for the magnitudes of the signals produced by nonlinear mixing in the fiber.

$l$ and transmitted pump and probe powers $P(\omega_1,l)$ and $P(\omega_2,l)$,

$$M=S(2\varepsilon_1-\varepsilon_2)-S(\varepsilon_1)-10\log_{10}P(\omega_1,l) -10\log_{10}P(\omega_2,l)-13al -10\log_{10}(e^{-al/2}-e^{-3al/2}) . \quad (56)$$

Here, $S(\varepsilon_i)\sim 10\log_{10}[P(\omega_i,l)P(\omega_{\rm LO})]$ is the spectrum-analyzer signal level in dBm at the indicated beat frequency, the powers are in watts, and the dependence on absorption $\alpha$ and fiber length $l$ normalized the figure of merit to the $\alpha l=$const case.

Typical results are shown in Table I for six fibers. The theory of 4WM in fibers relates our figure of merit $M$ to $K$ and to the nonlinear susceptibility $\chi^{(3)}$ and the mode area $A$,[25]

$$M=20\log_{10}K+19.79 =20\log_{10}\left[\frac{3\mu_0\omega_3}{n^2A\alpha}f_2\langle\chi^{(3)}\rangle\right]+19.79 . \quad (57)$$

The experimental 4WM coefficient $KP(\omega_1,0)$ is related to the coupling constant $\kappa$ in Eq. (30) by

$$KP(\omega_1,0)\approx\frac{0.102}{\alpha}\kappa|E|^2 \text{ when } \alpha l\ll 1 . \quad (58)$$

Since the nonlinear susceptibility of all these fibers should be equal and equal to that of fused silica, our results can be considered as measurements of the mode areas.[45] It is not surprising that the fibers with smaller modes give higher values of $M$ (and of the SBS gain).

From this information, we determined that the best fiber available to us was the Hitachi SP-6315. Unfor-

tunately, the GAWBS spectrum of this fiber (partly shown in Fig. 5) has wide and overlapping peaks with no regions at the quantum noise level.[42] The width of the GAWBS components is due to the damping provided by the jacket material. In later experiments, we hope to modify or remove the jacket or find an even more suitable fiber.

### B. Heterodyne detected four-wave parametric fluorescence

The ideas proposed previously in this paper are speculative enough that an early and concrete experimental test seems desirable to justify further effort. We have performed such an experiment and appear to have detected the increased noise or "unsqueezing" due to nondegenerate four-wave mixing in a fiber. The results are qualitatively consistent with expectations, but far from definitive. Still, the experiment highlights the actual difficulties that will be encountered in a squeezing experiment while providing sufficient results to encourage further effort.

The general scheme of the experiment is similar to Fig. 3. A stabilized single-mode krypton laser at 647 nm was coupled through a Faraday rotation isolator into a 100 m length of Hitachi SP-6315 single-mode fiber. The fiber was wrapped around an aluminum drum, the top of which could be heated to 300 °C while the bottom could be cooled down to liquid-nitrogen temperature. The output of the fiber was recollimated and directed into a specially constructed confocal Fabry-Perot interferometer.

The input mirror of the 10-cm spacing interferometer had 94% reflectivity, while the back-mirror reflectivity was 99.6%. The reflection from the input surface was directed into an EG&G FND-100 photodiode which was used for noise measurement. Other interferometer outputs were directed to a second photodetector used for servo control of the interferometer. The interferometer resonance frequency was locked to the laser frequency by dithering one mirror and integrating the difference between the lock-in-detected detector amplitude and a nominal set-point and then applying the integrated voltage to a piezoelectric translator on one mirror. The phase of the reflected light could be varied a bit by changing the reference level. The maximum excursion was too small to approach $\Phi=\pm\pi/4$, but the quadrature at $\Phi=0$ could be clearly accessed.

The noise-measurement photodiode produced two outputs. The steady-state dc current was measured by a digital ammeter to determine the detected optical power. The high-frequency detector output was amplified by a Q-bit 538 preamplifier and boosted further by a Minicircuit Laboratory ZHL-1-2W power amplifier. The amplifier outputs were then displayed on a Hewlett-Packard Model No. 8568B spectrum analyzer. When the dc detector current was 4 mA, corresponding to a detected power of 10 mW, the total (quantum plus thermal) noise level displayed on the spectrum analyzer was 3 dB above thermal noise alone.

The quantum noise level at every detector current was measured by shining an incoherent source on the detector, and measuring the current and noise level. The process was repeated using the krypton laser and the output of a short optical fiber. At low detected power, the noise was entirely thermal in origin. When the thermal noise level was subtracted from the total noise, the remaining quantum noise power varied linearly with the detector current as expected.

When the laser was coupled into the long fiber and the output reflected from the interferometer into the noise-detector diode, the GAWBS spectrum of the Hitachi fiber appeared on the spectrum analyzer. Adjusting the set-point of the cavity servo (and thus altering the phase of the local oscillator) resulted in a minimum GAWBS noise signal. This minimum GAWBS condition corresponds to a zero-average phase shift for the local-oscillator beam. The nonzero minimum deviation from the shot noise level results from servo error and oscillation which produces a nonzero mean-square phase shift.

The spectrum-analyzer frequency scan was stopped at a frequency of 47.8 MHz which corresponds to a minimum in the GAWBS spectrum. With maximum phase shift, the minimum GAWBS noise at this frequency was $\sim 5$ dB above the quantum plus thermal noise when the detector current was 4 mA. With zero-average phase shift, the GAWBS noise should be well below quantum noise at all our detector powers. Displaying the noise level as a function of time revealed an oscillating noise component that synchronized with the 60-Hz line frequency, indicating a line-frequency-induced servo error. Measurements of the noise level were therefore made at the minimum of the wave form.

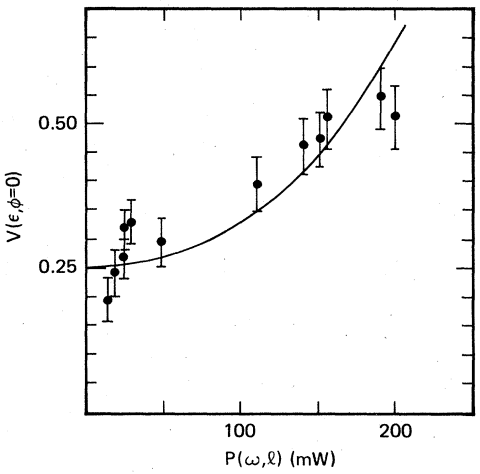


FIG. 8. Quadrature-variance increase due to heterodyne-detected four-wave parametric fluorescence measured in the apparatus of Fig. 3 on 100 m of Hitachi SP-6315 fiber. The points represent measurements of the noise level measured by the spectrum anlayzer relative to the noise produced by an incandescent light or unmixed laser beam yielding the same average detector current. The horizontal axis is the pump power at the output of the fiber. The solid curve is the prediction of Eq. (30) for the fiber parameters of Table I, and an effective interaction length of 83 m. Since the 1.4-dB attenuation of this fiber is greater than the optimum described in the text, one must correct the interaction length accordingly. Data taken at low pump power is uncertain because of the difficulty in correcting precisely for the thermal noise in the detection system.

In the four-wave-mixing experiment, the laser intensity coupled into the fiber was increased from 12 to 200 mW. The output of the fiber was reflected from the interferometer, but with a decrease in local-oscillator power of a factor of 10, making that beam weak enough to be detected without damaging the photodiode. The noise power measured at 47.8 MHz on the spectrum analyzer was recorded along with the dc detector current and pump power inside the fiber.

To reach a pump power of 200 mW inside the fiber without stimulated Brillouin scattering, one must impose a 400° temperature gradient along the fiber. The Hitachi fiber could tolerate the high and low temperatures only for limited time. Only two runs could be made before the fiber fractured. The results are presented in Fig. 8. The vertical axis shows the ratio for the detected noise in the four-wave-mixing experiment to the quantum noise level found for the thermal and laser light at the same detector current. The horizontal axis is the pump power at the output of the fiber. While there is a lot of scatter in the data, it does appear that four-wave mixing produces more noise than would be produced by a coherent state. The solid line shows the prediction of Eq. (30) for a value of $K$ implied by the measurement in Table I. This value of $K$ implies a value for $\kappa |E|^2 l$ of 0.83 for $P(\omega_1,l)=200$ mW. The open rectangles in Fig. 1 correspond to this value of $\kappa |E|^2 l$. This result is very encouraging, given the limitations of the experiment. If one were able to phase shift the local oscillator by 45° without encountering GAWBS, squeezing by a factor of 5 might well appear.

## ACKNOWLEDGMENTS

We would like to thank Dr. John Hall and Dr. Roger Stolen for the loan of valuable apparatus and samples. This research was partly supported by the U. S. Office of Naval Research, Department of the Navy, under Contract No. N00014-82-C-0694.

*Permanent address: Institut d'Optique, Orsay, France.

[1]For a review, see D. F. Walls, Nature **306**, 141 (1983).

[2]H. P. Yuen, Phys. Rev. A **13**, 2226 (1976).

[3]C. M. Caves, Phys. Rev. D **23**, 1693 (1981).

[4]J. H. Shapiro, P. Kumar, and M. W. Maeda, J. Opt. Soc. Am. **1B**, 517 (1981).

[5]R. E. Slusher, B. Yurke, and J. F. Valley, J. Opt. Soc. Am. **1B**, 525 (1984).

[6]M. D. Levenson, J. Opt. Soc. Am. **1B**, 525 (1984).

[7]L. A. Lugiato and G. Strini, Opt. Commun. **41**, 374 (1982).

[8]M. D. Reid and D. F. Walls, Phys. Rev. A **28**, 332 (1983).

[9]G. J. Milburn and D. F. Walls, Opt. Commun. **39**, 401 (1981).

[10]L. A. Lugiato and G. Strini, Opt. Commun. **41**, 67 (1982).

[11]L. Mandel, Opt. Commun. **42**, 437 (1982).

[12]L. A. Lugiato, G. Strini, and F. de Martini, Opt. Lett. **8**, 256 (1983).

[13]N. Bloembergen, *Nonlinear Optics* (Benjamin, New York, 1966).

[14]H. P. Yuen and J. H. Shapiro, Opt. Lett. **4**, 334 (1979).

[15]R. S. Bondurant, P. Kumar, J. H. Shapiro, and M. Maeda, Phys. Rev. A **30**, 343 (1984).

[16]G. J. Milburn, M. D. Levenson, and D. F. Walls, J. Opt. Soc. Am. **1B**, 390 (1984).

[17]P. Kumar and J. H. Shapiro, Phys. Rev. A **30**, 1568 (1984).

[18]M. D. Reid and D. F. Walls, Opt. Commun. **50**, 406 (1984).

[19]J. Perina, V. Perinova, C. Sibilia, and M. Bertolotti, Opt. Commun. **49**, 285 (1984).

[20]J. Jansky and Y. Yushin, Opt. Commun. **49**, 290 (1984).

[21]M. D. Reid and D. F. Walls, Phys. Rev. A **31**, 1622 (1985).

[22]M. J. Collett and C. W. Gardiner, Phys. Rev. A **30**, 1386 (1984).

[23]B. Yurke, Phys. Rev. A **29**, 408 (1984).

[24]L. B. Jeunhomme, *Single Mode Fiber Optics* (Dekker, New York, 1983).

[25]K. O. Hill, D. C. Johnson, B. S. Kawasaki, and R. I. MacDonald, J. Appl. Phys. **49**, 5098 (1978).

[26]R. H. Stolen and J. E. Bjorkholm, IEEE J. Quantum Electron. **QE-18**, 1062 (1982).

[27]W. H. Louissell, *Radiation and Noise in Quantum Electronics* (McGraw-Hill, New York, 1964).

[28]H. P. Yuen and V. W. S. Chan, Opt. Lett. **8**, 177 (1983); **8**, 345 (1983).

[29]B. L. Schumaker, Opt. Lett. **9**, 189 (1984).

[30]B. L. Schumaker and C. M. Caves, in *Coherence and Quantum Optics V*, edited by L. Mandel and E. Wolf (Plenum, New York, 1984), pp. 743–750.

[31]C. M. Caves and B. L. Schumaker, Phys. Rev. A **31**, 3068 (1985); B. L. Schumaker and C. M. Caves, *ibid.* **31**, 3093 (1985). Caves and Schumaker have introduced the following non-Hermitian operators describing the quadrature phase amplitude at frequency $\varepsilon$: $X_1'=(a_2+a_3^\dagger)/\sqrt{2}$, $X_2'=(a_2-a_3^\dagger)/\sqrt{2}i$. Defining the variances of these non-Hermitian operators as $V(X_i')=\frac{1}{2}\langle X_i' X_i'^\dagger + X_i'^\dagger X_i'\rangle - \langle X_i'\rangle\langle X_i'^\dagger\rangle$, we find $V(X_i')=2V(X_i)$, however, our condition for squeezing is $V(X_i)<\frac{1}{4}$ and the "squashing" of Caves and Schumaker is $V(X_i')<\frac{1}{2}$ so that both definitions give identical results.

[32]K. Wodkiewicz and M. S. Zubairy, Phys. Rev. A **27**, 2003 (1983).

[33]M. D. Reid and D. F. Walls (unpublished).

[34]M. D. Levenson, *Introduction to Nonlinear Laser Spectroscopy* (Academic, New York, 1982).

[35]M. V. Klein, *Optics* (Wiley, New York, 1970), pp. 205–212.

[36]P. Connes, J. Phys. Radium **19**, 262 (1958).

[37]S. C. Rashleigh and R. H. Stolen, Laser Focus **19**, 155 (1983), and references therein.

[38]E. P. Ippen and R. H. Stolen, Appl. Phys. Lett. **21**, 539 (1972).

[39]Y. R. Shen, *The Principles of Nonlinear Optics* (Wiley, New York, 1984), Chap. 11.

[40]R. Vacher and J. Pelous, Phys. Rev. B **14**, 823 (1976).

[41]R. M. Shelby, M. D. Levenson, and P. W. Bayer, Phys. Rev. Lett. **54**, 939 (1985).

[42]R. M. Shelby, M. D. Levenson, and P. W. Bayer, Phys. Rev. B **31**, 5244 (1985).

[43]A. Lane, P. Tombesi, H. J. Carmichael, and D. F. Walls, Opt. Commun. **48**, 155 (1983).

[44]R. W. P. Drever, J. L. Hall, E. V. Kowalsky, H. Hough, G. M. Ford, A. J. Monley, and H. Ward, Appl. Phys. B **31**, 97 (1983).

[45]Y. R. Shen, *The Principals of Nonlinear Optics* (Wiley, New York, 1984), Chap. 26.